KINETIC STUDIES ON PHOTOLYSIS-INDUCED GELATION OF SICKLE CELL HEMOGLOBIN SUGGEST A NEW MECHANISM

F. A. Ferrone, J. Hofrichter, H. R. Sunshine, and W. A. Eaton, *Laboratory of Chemical Physics, National Institute of Arthritis, Metabolism and Digestive Diseases, National Institutes of Health, Bethesda, Maryland 20205 U.S.A.*

ABSTRACT The kinetics of deoxyhemoglobin S gelation have been investigated using photolytic dissociation of the carbon monoxide complex to initiate the process. Measurements over a wide range of times, 10^{-3}–10^{4} s, show that both the concentration dependence of the tenth-time (i.e., the time required to complete one-tenth the reaction) and the time dependence of the process decrease as gelation speeds up. In slowly gelling samples, where single domains of polymers are formed in the small sample volumes employed with this technique ($1–2 \times 10^{-9}$ cm^3), there is a marked increase in the variability of the tenth-times. These results are explained by a mechanism in which gelation is initiated by homogeneous nucleation of polymers in the bulk solution phase, followed by heterogeneous nucleation on the surface of existing polymers. At the lowest concentrations, homogeneous nucleation is so improbable that stochastic behavior is observed in the small sample volumes, and heterogeneous nucleation is the dominant pathway for polymer formation, thereby accounting for the high time dependence. At the highest concentrations homogeneous nucleation becomes much more probable, and the time dependence decreases. The decrease in concentration dependence of the tenth-time with increasing concentration results from a decrease in size of both the homogeneous and heterogeneous critical nuclei. The model rationalizes the major observations on the kinetics of gelation of deoxyhemoglobin S, and is readily testable by further experiments.

INTRODUCTION

In this paper we present the results of an investigation of the kinetics of deoxyhemoglobin S gelation, initiated by photolysis of the carbon monoxide complex. With this technique it is possible to study gelation at previously inaccessible times and concentrations. Several new features of the process emerge from this study, which lead us to formulate a new mechanism for gel formation. The mechanism postulates two pathways for polymer formation: homogeneous nucleation of polymers in the bulk solution phase, as previously proposed, and heterogeneous nucleation of polymers on the surface of existing polymers.

During the past several years, there have been a number of important advances in elucidating the structure of the hemoglobin S gel and the mechanism of its formation (1–3). Optical birefringence (4, 5), electron microscopy (6–8), and sedimentation studies (9, 10) have shown that at equilibrium a gel of deoxyhemoglobin S contains an ordered polymer phase, which behaves thermodynamically very much like a protein crystal, and a solution phase consisting of monomeric (i.e., 64,000 mol wt) hemoglobin. The concentration of deoxyhemoglobin S in the solution phase may therefore be regarded as a solubility with respect to the polymer phase (5, 11–13). Because the solubility of deoxyhemoglobin S is so

Dr. Ferrone's present address is the Department of Physics and Atmospheric Science, Drexel University, Philadelphia, Pennsylvania 19104

high (>16 g/dl), the solution phase is highly nonideal. However, the large nonideality can be completely accounted for by the hard sphere excluded volume effects of the protein (14, 15). There is very little information on the arrangement of the polymers in the gel, but there is now a considerable amount of data on the structure of the individual polymers. From image reconstruction of electron micrographs a model for the polymer has been derived which consists of 14 helical strands (16). A combination of fiber x-ray diffraction on gels (17) and studies on mutants (18) has suggested that at least some of the intermolecular contacts found in the deoxyhemoglobin S crystal are also present in the polymer.

Most of the information on the mechanism of gel formation has come from measurements of kinetic progress curves for a variety of solution conditions. The progress curve is characterized by a pronounced delay, during which no signal change is detectable using many different physical techniques, followed by an explosive autocatalytic appearance of polymer (19–24). There is a marked sensitivity of the delay time, t_d, to the solution composition and temperature, which can be summarized by the approximate empirical relation (12, 19, 25):

$$1/t_d \propto S^n, S \equiv c_0/c_s, \tag{1}$$

where the supersaturation, S, is defined as the initial total hemoglobin concentration, c_0, divided by the equilibrium solubility, c_s. The exponent n has been found to vary between 30 and 50 (12, 19, 25, 26). To explain these findings, it was previously proposed that the delay time is controlled by the rate of homogeneous nucleation of individual polymers, and that polymers are formed by simple bimolecular addition steps (19, 25), i.e.,

$$\begin{aligned}
M + M &\rightleftharpoons M_2 \\
M + M_2 &\rightleftharpoons M_3 \\
&\vdots \\
M + M_{i-2} &\rightleftharpoons M_{i-1} \\
M + M_{i-1} &\rightleftharpoons M_i \\
&\vdots \\
M + M_j &\rightleftharpoons M_{j+1}
\end{aligned} \tag{2}$$

There are competing thermodynamic forces in such an aggregation scheme which produce a free energy barrier to polymer formation (27, 28). The net loss of translational and rotational entropy disfavors aggregation, while the formation of intermolecular bonds favors aggregate formation. Initially, the loss of translation and rotational entropy dominates and aggregation is thermodynamically unfavorable (as indicated by the relative length of the arrows for the elementary chemical steps). As the aggregate grows there is an increase in the number of bonds per molecule, which makes aggregation more and more favorable. At some point addition of monomer becomes thermodynamically favorable, and monomers add endlessly until the solubility is reached. The thermodynamically least stable species in the system for a given supersaturation is often referred to as the critical nucleus (the $(i-1)$-mer). The critical nucleus need not have any special structure and we have assumed that it is simply a piece of the infinite polymer. Furthermore, the size of the critical nucleus depends on the supersatura-

tion and is continuously increasing during the course of aggregation as the supersaturation decreases from depletion of monomer. For purposes of discussion, we consider nucleation to include all those steps up to and including formation of the critical nucleus, while growth of polymers includes all subsequent steps.

To obtain an analytical expression for the delay time with this kinetic scheme, a model was previously developed with three important simplifying assumptions (29). First, the size of the critical nucleus was assumed to be constant over the range of supersaturation employed in the experiments; second, the critical nucleus was assumed to be in constant equilibrium with monomer from time zero; and third, the addition of monomers to the critical nucleus and all subsequent growth steps were considered to be irreversible. The large solution phase nonideality was also included in the theory by including concentration dependent activity coefficients for the monomer and the nucleus activated complex. The equilibrium assumption was motivated by the experimental connection between the delay time and the solubility, while the irreversible growth assumption restricted comparison of theory and experiment to the early phase of the reaction. This equilibrium nucleation/irreversible growth model was successful in explaining the dependence of the delay time on initial concentration and solubility, as well as the activation energy and the temperature dependence of the activation energy. An interesting result of the theory was that the major part of the dependence of the delay time on supersaturation arises from the concentration dependence of the monomer activity coefficient. More recently, the theory was extended to mixtures of deoxyhemoglobin S with normal and fetal deoxyhemoglobins, using results from solutibility studies to obtain thermodynamic parameters for nucleus formation (30). The model quite adequately accounted for both the composition dependence of the delay time at constant total hemoglobin concentration and the concentration dependence of the delay time at constant composition.

Despite its successes, the theory has remained incapable of explaining the extreme autocatalysis in the early portion of the progress curves. The theory predicts an onset of polymerization no greater than 2nd order in time, whereas the first 10% of the reaction proceeds as the 10th to 20th power of time (29). The inability of the theory to predict the shape of the progress curve correctly is a severe deficiency, and might suggest that the mechanism is fundamentally incorrect. Because of its successes, we adopted the view that equilibrium nucleation is an essential part of the mechanism, but that some process in addition to individual fiber nucleation is responsible for the extreme autocatalysis (29, 31). With this assumption, we were motivated to extend the kinetic measurements to as short a time as possible, with the aim of separating the overall process into its components.

The basic experimental objective then, was to develop a kinetic method in which initiation was fast and which had a wide dynamic range. All of the previous kinetic experiments had been performed by inducing gelation thermally, taking advantage of the characteristic property of hemoglobin S that between 0° and 37°C gelation is favored by increased temperature. The techniques employed in these studies, however, were limited to delay time measurements of tens of seconds or longer. We turned to photolysis of the carbon monoxide complex as a means of rapidly creating and maintaining deoxyhemoglobin S at a constant temperature. Carbon monoxide, moreover, recombines rapidly in the dark, permitting repetitive experiments. With this method we have been able to measure delay times as short as milliseconds (31).

In the work described below, we have used an argon ion laser as both a photolysis source and a light scattering probe source to investigate the gelation of deoxyhemoglobin S in the time range 10^{-3}–10^{4} s, the concentration range 20–40 g/dl, and the temperature range

5°–50°C. Several principal new results emerge from this investigation. At the shortest times the progress curves are much less autocatalytic and are closer to the shape predicted by the simple nucleation theory described above. The concentration dependence also decreases with decreasing delay time. Finally, at long times, where single domains of polymers are formed, the delay times become highly variable, while the post-delay growth rate remains the same. These observations have suggested a mechanism in which gelation is initiated by homogeneous nucleation of polymers in the bulk solution phase followed by the heterogeneous nucleation of polymers on the surface of existing polymers. Heterogeneous nucleation is responsible for the extreme autocatalysis at long times, while homogeneous nucleation becomes increasingly important at shorter times, thereby explaining the decreased time dependence. By formulating an explicit model for the free energy barrier to polymer formation for both nucleation processes, the decrease in concentration dependence with increasing supersaturation is explained as arising from a decrease in the size of both homogeneous and heterogeneous nuclei.

METHODS AND MATERIAL

The major problem in implementing a steady-state photolysis technique is the large temperature rise associated with the absorption of sufficient light to photolyze continuously a concentrated hemoglobin sample. Since heating occurs in the bulk of the sample whereas cooling occurs at the surface, it is important to maximize the surface to volume ratio of the illuminated volume. Consequently, we employed a focused laser and a microspectrophotometer to achieve photodissociation with miminal heating on sample volumes between 10^{-9} and 2×10^{-9} cm^3.

The microspectrophotometer used for optical absorption and kinetic measurements is described in detail elsewhere (reference 32 and footnote 1). The 514-nm line of a Spectra-Physics model 166 argon ion laser (Spectra-Physics Inc., Laser Products Division, Mountain View, Calif.) was used as both a source for photolysis and for light scattering, which was used to monitor the gelation process. The beam was incident on the sample at ~45°, and was focused to produce an illuminated ellipse of $\sim 25 \times 35$ μm. Optical absorption and light scattering measurements were made on a circular region ~6 μm in diameter in the center of the illuminated area. Temperature was controlled via a Cambion thermoelectric stage and a controller of our own design. Operation below the dew point was made possible by a nitrogen flow system.

Concentrated oxyhemoglobin S was prepared as described by Sunshine et al. (30). After the last dialysis against 0.15 M potassium phosphate, pH 7.3, the concentrated oxyhemoglobin stock solution was saturated with carbon monoxide. A range of concentrations was obtained by serial dilution of this stock solution with CO-saturated phosphate buffer. Concentrations of the final solutions were determined in triplicate as cyanmethemoglobin using an extinction coefficient of 10,900 M^{-1} cm^{-1} for the 542-nm peak and a molecular weight of 16,100/heme. Before storage in sealed tubes, 1 M sodium dithionite in CO-saturated buffer was added to produce a final dithionite concentration of 0.055M. The samples were stored at 4°C under a CO atmosphere. For kinetic measurements, a 2–4 μm layer of solution was prepared between two coverslips, and the sealed with Kerr sticky wax. All sample manipulations were performed under a water-saturated CO atmosphere.

To establish the power densities required to achieve full photolysis, control experiments were done on a sample of hemoglobin A prepared in a similar fashion to the hemoglobin S. The power densities required depend upon the recombination rates with which they must compete, and these rates in turn depend on the local concentration of carbon monoxide. Since the highest concentrations of hemoglobin employed bind ~24 times more carbon monoxide than is carried free in solution, photolysis is followed by a high local concentration of CO, which then diminishes as the CO diffuses into the unilluminated regions of the sample. In a series of experiments designed to determine the kinetics of photolytic initiation, we established that simple radial diffusion described this process well, and that for our

[1]Ferrone, F. A., J. Hofrichter, and W. A. Eaton. Manuscript submitted for publication.

geometry <3% of the CO has diffused away in the first 10 ms. To guarantee complete photolysis at the highest recombination rates, we measured the level of dissociation within the first 10 ms for a 40 g/dl sample. This experiment set the power level needed for full photolysis. From measurements of the power incident on the sample and the beam profile, the required average power density was estimated to be 3 kW/cm^2. The temperature rise was measured on a cresol red solution in Tris buffer, which has a strongly temperature dependent absorption spectrum, and was found to be ~4°C at 3 kW/cm^2. However, for each sample studied, we established that full photolysis had been obtained, and measured the temperature rise by an independent method described in detail below.

Gelation was monitored by measuring the scattered light collected by a ×32 superstage objective with a 0.4 numerical aperature, and projected through a ×10 eyepiece onto a photomultiplier tube. Kinetic data were recorded on a Nicolet Explorer digital oscilloscope (Nicolet Scientific Corp., Northvale, N. J.), and stored on magnetic tape via a Hewlett-Packard 9825 calculator (Hewlett-Packard Co., Palo Alto, Calif.)

RESULTS

Kinetic data were collected on samples at nine concentrations, ranging from 21.8 to 39.3 g/dl and ambient temperatures between 5° and 39.5°C. Fig. 1 shows typical progress curves for samples with delay times ranging from 20 ms to ~10 s. The shape of the curves changes considerably with changing delay time, exhibiting a much more abrupt onset of gelation at longer times. To describe the initial part of the progress curves quantitatively, the first 15% of the signal change was fit with the function:

$$f = (t/\tau)^{\alpha}, \tag{3}$$

where f is the fraction of signal change relative to the peak scattered intensity, t is time, and τ, and α are fitting parameters. From α and τ a tenth-time, $t_{1/10}$, the value of t at $f = 0.1$, was calculated and was used throughout the analysis as the characteristic time for the reaction. Comparison of light scattering data on large sample volumes with calorimetric and birefringence data justifies the assumption that the signal change is linearly proportional to the fractional conversion of monomer into polymer.

To determine the temperature corresponding to each laser power density and ambient temperature, the following procedure was employed. For each setting of the ambient temperature, i.e., the temperature of the thermostat, the kinetics were measured at several laser power densities above that necessary to achieve complete photolysis. The ambient temperature was changed and the process repeated. This procedure generated a family of curves of tenth-time vs. ambient temperatures at different laser power densities (Fig. 2). To

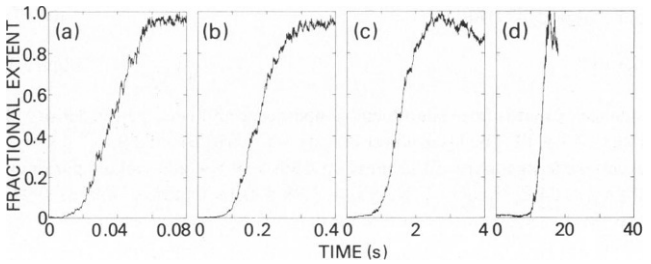

Figure 1 Kinetic progress curves. In each panel, the intensity of scattered light normalized to the peak scattered intensity is shown as a function of time. The concentrations and true temperatures for each panel are as follows: (*a*) c = 35.2 g/dl, T = 34.8°C; (*b*) c = 35.2 g/dl, T = 23.5°C; (*c*) c = 26.9 g/dl, T = 35.2°C; (*d*) c = 26.9 g/dl, T = 23.6°C. Note the increasing abruptness of the reaction as the characteristic time increases.

calculate the true temperature for each ambient temperature and laser power density, we assume that the apparent activation energy, E_a, contained a term proportional to temperature, i.e., that

$$E_a = R\frac{\mathrm{d}\ln t_{1/10}}{\mathrm{d}(1/t)} = E - CT, \tag{4}$$

where $t_{1/10}$ is the tenth-time, T is the true temperature, R is the gas constant, and E and C are temperature-independent constants. The integrated form of Eq. 4 is:

$$\ln t_{1/10} = \frac{E/R}{T_a + \beta P} - \frac{E/R}{273} + \frac{C}{R}\ln\left(\frac{T_a + \beta P}{273}\right) + \ln t_{1/10}^{273}, \tag{5}$$

where we have explicitly written the true temperature T, as a sum of the ambient temperature, T_a, plus the increase in temperature resulting from laser heating. This temperature increase is assumed to be linerly proportional to laser power density, and is written as βP, where β is a heating coefficient and P is the power density. The constant of integration is chosen to be the tenth time at ice temperature $t_{1/10}^{273}$. Eq. 5 was used to obtain a least squares fit to a data set consisting of tenth-times as a function of ambient temperature and power density, thereby determining the E, C, β, and $t_{1/10}^{273}$. The theoretical curves in Fig. 2 were drawn with Eq. 5, using the parameters from the least squares fit. The true temperature for each set of experimental conditons is determined by β, which was typically 1.2°C/kW/cm^2 for a sample with an optical density of 0.029 at 514 nm (corresponding to an optical density at the 419-nm

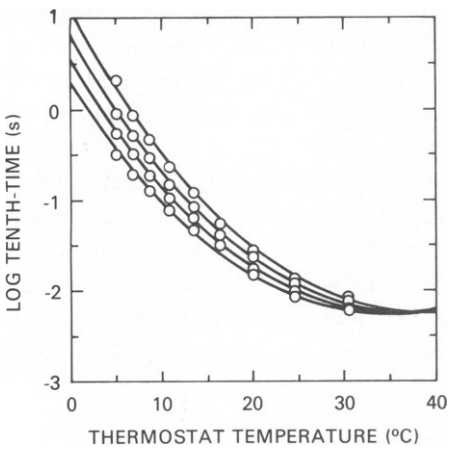

Figure 2

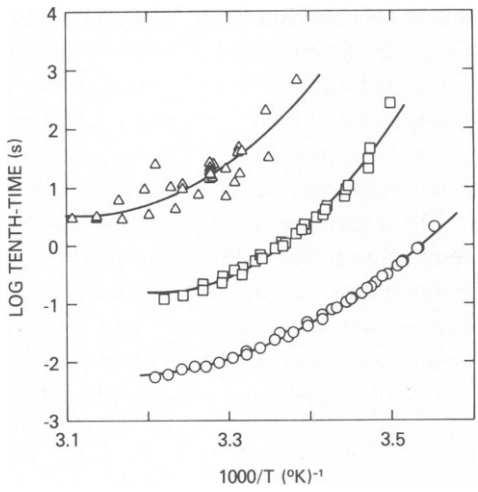

Figure 3

Figure 2 Dependence of tenth-time on ambient temperature and laser power density. The concentration of hemoglobin S was 37.3 g/dl. The laser power density was varied from 2.9 to 7.4 kW/cm^2 in steps of 1.5 kW/cm^2. The curves are least squares fit to the data using Eq. 5 which yielded parameters E = 264 ± 11 kcal/mol., C = 0.83 ± 0.04 kcal/mol − °K, $t_{1/10}^{273}$ = 3.88 ± 0.12 s and β = 1.05 ± 0.04°C/kW/cm^2. The latter value corresponds to a temperature difference of 1.5°C between adjacent curves. Sample absorbance at 514 nm was 0.029.

Figure 3 Arrhenius plots for three different concentrations. Each curve is the condensation of a family of curves similar to that shown in Fig. 2. The circles are the data shown in Fig. 2. The triangles are data for a concentration of 24.8 g/dl, with absorbance at 514 nm of 0.036; the best fit to Eq. 5 gave E = 420 ± 110 kcal/mol, C = 1.3 ± 0.36 = kcal/mol − °K, $t_{1/10}^{273}$ = 19 ± 3 s, and β = 2.2 ± 0.3°C/kW/cm^2. For the squares, the concentration was 29.0 g/dl, the absorbance at 514 nm was 0.035, and the best fit gave E = 570 ± 60 kcal/mol, C = 1.8 ± 0.2 kcal/mol − °K, $t_{1/10}^{273}$ = 14.0 ± 0.7 s and β = 1.5 ± 0.9°C/kW/cm^2.

Soret peak of 1.0). This value agreed well with the heating coefficient of 1.4°C/kW/cm^2 determined from the control experiments with the cresol red temperature indicator.

Fig. 3 shows the data of Fig. 2 replotted as tenth-time vs. the reciprocal absolute temperature, calculated as described above. Also shown are the data from two lower concentrations, 29.0 and 24.8 g/dl. As was found previously for thermally-induced gelation kinetics, the apparent activation energy decreases with increasing temperature. The data also suggest that at a fixed temperature the activation energy is decreasing with increasing initial concentration.

The concentration dependence of the tenth-time at 20° and 35°C is shown in Fig. 4. The points in Fig. 4 were obtained from the parameters used to fit the data on the temperature dependence of the tenth-time. Between 10^2 and 10^3 s, we find a concentration dependence of ~30th order at 20°C, in good agreement with the values of 30–50 found previously using the thermal induction method to study gelation kinetics (12, 19, 26, 30). It is apparent in Fig. 4 that at the higher concentrations, which were not accessible to study by the thermal induction method, the dependence is decreasing significantly. Using the four points with the longest tenth-times, the concentration dependence is 26th power at 20°C and 21st power at 35°C, while the corresponding values calculated from the four points with the shortest tenth-times are 17th and 13th power.

As we noted for the data in Fig. 1, the time dependence in the initial phases of the reaction increases with increasing tenth-time. This increase occurs whether the tenth-time is increased by decreasing concentration or temperature. In Fig. 5 the time dependence, as expressed by the parameter α in Eq. 3, is plotted vs. tenth-time. Not only does α begin to increase markedly

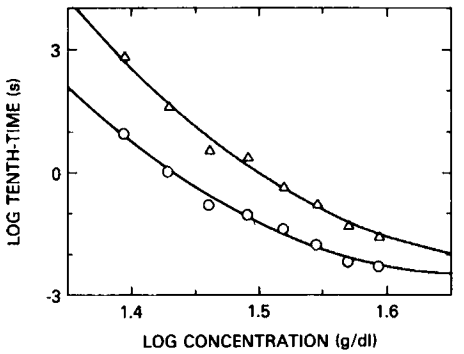

Figure 4

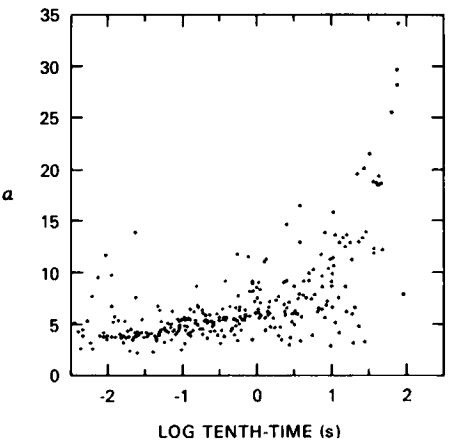

Figure 5

Figure 4 Concentration dependence of tenth-times. The points are calculated from the curves fit to data similar to that of Fig. 3. The triangles are calculated for a temperature of 20°C, the circles for 35°C. The curves are the best fit of a sum of constant, linear and quadratic terms. The slope between the slowest two points at 20° is 25, and 20 for 35°. The slope for the slowest four points at 20° is 26, and 21 for 35°. The slope for the fastest four points at 20° is 17, and 13 at 35°. The slope of the fit curves, at log c = 1.35 is 35 for 20°, and 29 for 35°.

Figure 5 Time dependence. Data at all temperatures and concentrations studied was parameterized according to Eq. 3, and the values of α are shown here as a function of log of tenth-times. To show the increasing variability of α, it was necessary to exclude some of the data with high α values: ten points have been omitted with α values of 34, 37, 43, 49, 52, 75, 80, 110, 122, and 189, at abscissa values of 1.96, 2.02 1.82, 1.73, 2.34, 2.19, −2.1, 2.85, 2.00, and 2.88, respectively. The increase in variability at the shortest times arises from instrumental imprecision.

for progress curves with tenth-times $\gtrsim 1$ s, but the variability increases as well. The slight increase in variability at the shortest times is attributed to decreased signal-to-noise. An increased variability in tenth-time at longer times is also apparent in the data in Fig. 3. This was surprising, because the precision was expected to be best for the longer experiments, both because of improved signal-to-noise and because CO diffusion out of the illuminated volume guarantees complete photolysis. As a further measure of the decreased reproducibility of tenth-times with increasing time, data taken under identical conditions were compared. By identical conditions we mean that neither the laser power nor ambient temperature was changed, nor was the sample moved, so that the sample part of the solution was used for repeated measurements. The results of these comparisons are shown in Fig. 6, where the fractional deviation from the mean is plotted vs. the mean tenth-time. At tenth-times longer than ~1 s the reproducibility decreases dramatically.

Although the tenth-time becomes highly variable at longer times, the shape of the progress curve is not altered once gelation has begun. Fig. 7 shows progress curves measured under identical experimental conditions. The tenth-times differ by a factor of ~20, yet the initial shapes of the curves are virtually identical.

DISCUSSION

The principal new results on gelation kinetics from the photolysis technique were made possible by the large dynamic range and the increased spatial resolution of the method. For tenth-times >100 s, the concentration dependence is ~30th power (Fig. 4), in good agreement with the values observed in previous kinetic studies in the same time range, in which a temperature increase was used to induce gelation. In the same range, the time dependence, as parameterized by α in Eq. 3, is also large, with α values ranging between 40 and 190. In previous experiments, using sample volumes 10^5–10^9 times larger, the time dependence varied between 10th and 20th power (19, 25). In the newly accessible time range of 10^{-3}–1 s, both the concentration and time dependence are significantly decreased (Figs. 4 and 5).

A striking new result, which gives considerable insight into the mechanism of gelation, is that there is much more variability in the long tenth-times than in the short tenth-times (Fig.

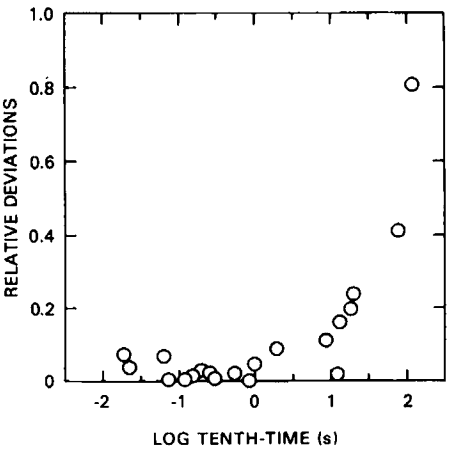

Figure 6 Best-case reproducibility. The fractional deviation from the mean tenth-time is shown as a function of log of mean tenth-time for experiments in which temperature, laser power, and sample position were identical.

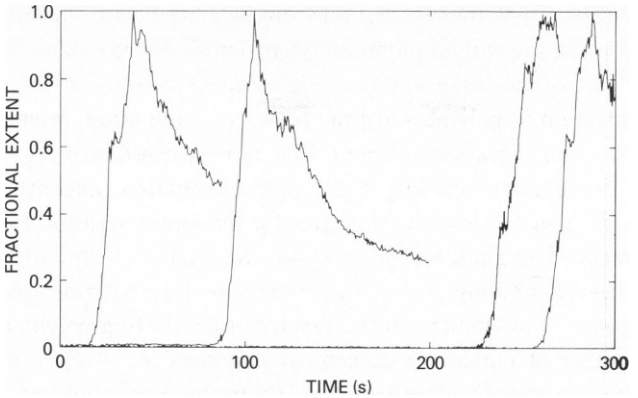

Figure 7 Comparison of tenth-time variability and variability of growth. Four sequential, identical kinetic experiments are shown. Although the curves begin at radically different times, the growth rate, once begun, is almost identical. Sample concentration was 31.0 g/dl; ambient temperature was 6.8°C. The slowest curve was obtained first, the fastest curve was obtained third. Each curve, including the slowest, was obtained after a 5-min wait after the end of a previous gelation experiment.

6). An important clue to the significance of this result is that the gels with tenth-times longer than ~10 s which were formed in a photolysed volume of $\sim 10^{-9}$ cm^3, appeared to consist of a single spherulitic domain when viewed between crossed linear polarizers. In contrast, gels formed with tenth-times $\lesssim 10^{-1}$ s contained domains too numerous to resolve optically. These observations on the optical structure of domains of polymers suggest that the variability at long times results from the control of gelation by a small number of events, and that we are observing the probability distribution for the occurrence of these events. A comparison of the progress curves in Fig. 7 supports this suggestion. The observation that the progress curves do not change as the tenth-time is changing, i.e., that they are superimposable when translated along the time axis, could be explained by postulating that a reproducible sequence of kinetic events, which results in the formation of a single domain of polymers, is initiated by a single molecular event. Since polymers contain on the order of 10^4 hemoglobin S molecules, a single domain in our experiments contains on the order of 10^4 polymers. If the initiating event is the nucleation of individual polymers, then we must find a mechanism which predicts the 10^4-fold proliferation of the number of polymers in the formation of a single domain. Since proliferation of polymers produces autocatalysis, such a mechanism could also explain the high time dependence. However, the mechanism of proliferation must also be compatible with a large concentration dependence of the tenth-time, suggesting that the additional polymers must also be formed by a nucleation process. We therefore propose a mechanism in which the initiating event for gel formation is the homogeneous nucleation of single polymers, followed by the heterogeneous nucleation of polymers on the surface of existing polymers.

The rate equations which contain both homogeneous nucleation and heterogeneous nucleation on the surface of polymers are (29):

$$\frac{dc_p}{dt} = K_N k_+ (\gamma c)^n + K_M \phi k_+ (c_0 - c)(\gamma c)^m \tag{6a}$$

$$-\frac{dc}{dt} = nK_N k_+ (\gamma c)^n + mK_M \phi k_+ (c_0 - c)(\gamma c)^m + (k_+ \gamma c - k_-)c_p. \tag{6b}$$

The first term in Eq. 6a is the rate of polymer formation by homogeneous nucleation while the

second term is the rate of polymer formation from heterogeneous nucleation. In Eq. 6b, the first two terms represent the rate of monomer incorporation into nuclei, while the third term corresponds to the rate of monomer addition and removal from polymers. In these equations, the number concentration of polymers at time t is c_p; c_0 is the initial monomer concentration; and c is the monomer concentration at time t. The activity coefficient for the monomer in the solution phase, γ, is necessary because of the high hemoglobin concentrations (14, 15, 29). The rate constants k_+ and k_- describe the rates for monomer addition to and removal from the growing polymers. The equilibrium constants K_N and K_M refer to the formation of a homogeneous nucleus containing $n - 1$ monomers in free solution and a heterogeneous nucleus containing $m - 1$ monomers on the surface of an existing polymer. The parameter ϕ scales the total number of monomers present as polymers $(c_0 - c)$ to give the number of effective sites for heterogeneous nucleation. In writing these equations we have assumed: (*a*) that the rate constants k_+ and k_-, for all polymer species are identical; (*b*) that nuclei are in continuous equilibrium with monomer so that the nucleation rate constants become the products, $K_N k_+$ and $\phi K_M k_+$; and (*c*) that the rate of heterogeneous nucleation is proportional to the total number of hemoglobin molecules present as polymers $(c_0 - c)$. This approximation is equivalent to assuming that polymers are dilute, long, and linear, in which case their surface area is directly proportional to their mass.

To resolve the coupled differential Eqs. 6a and 6b, we must specify values of K_N, K_M, n, m, ϕ, k_+, and k_-. Because the size of the critical nuclei depends on the supersaturation in the solution phase (c/c_s), the nucleus sizes, $(n - 1)$ and $(m - 1)$, and the equilibrium constants K_N and K_M, are continuous functions of the monomer concentration, c. Our first problem, then, is to develop a functional relation between these variables and the monomer concentration. This is equivalent to formulating a thermodynamic model for the free energy barrier to polymer formation, i.e., the free energy of an aggregate as a function of the number of molecules in the aggregate. To do so, we have chosen the simplest structural pathway for nucleation that retains the qualitative features of what is presently known about the polymer and gel structure. We have adopted a model in which all intermolecular bonds (contacts) have equal free energies of formation and aggregates of all sizes have the most compact structure.

In the Appendix we derive expressions for the equilibrium constants, K_N and K_M, as a function of n and m in terms of the various contributions to the chemical potential of the monomer, nucleus, and infinite polymer. The monomer chemical potential is divided into contributions from the free energy arising from translation of the center of mass, free energy from rotation of the entire molecule treated as a rigid body, and the internal free energy. The ideal gas equations are used to calculate the translational and rotational free energies (Table I). In the aggregates there are additional terms due to intermolecular bonding and relative motions of the centers of mass of the bonded molecules. These latter motions replace the translational and rotational degrees of freedom lost by monomers upon aggregation, and are treated as lattice vibrations. The free energy associated with these lattice vibrations is calculated using the Einstein approximation for a monatomic solid and the classical partition function (Table I).

The functions for the equilibrium constants (see Eqs. A7 and A8 of the Appendix) contain only three free parameters. One is the effective Einstein lattice frequency, ν_E (Table I); the second is the number of additional intermolecular bonds per monomer resulting from the bonding between a heterogeneous nucleus and an existing polymer, and is expressed by the parameter A' in Eq. A9 of the Appendix; the third parameter, μ_{NS}, expresses the difference in the lattice vibrations of a nucleus and infinite polymer arising from the additional surface

TABLE I

TRANSLATIONAL (T), ROTATIONAL (R), AND VIBRATIONAL (V) CONTRIBUTIONS TO THE CHEMICAL POTENTIAL (μ) OF THE HEMOGLOBIN MONOMER (S), NUCLEUS (N), AND POLYMER (P)

$$\mu_{ST} = -kT\left[\ln\left(\frac{2\pi MkT}{h^2}\right)^{3/2} + 1 - \ln\frac{N_0}{V_0}\right] = -18.988 \text{ kcal/mol}$$

$$\mu_{SR} = -kT \ln\frac{\pi^{1/2}}{\sigma}\left(\frac{8\pi^2 IkT}{h^2}\right)^{3/2} = -17.14 \text{ kcal/mol}$$

$$\mu_{NT}(j) = -3/2\, kT \ln(j) + \mu_{S_T}$$

$$\mu_{NR}(j) = -3/2\, kT \ln\left[\frac{I(j)}{I}\right] + \mu_{SR} = -5/2\, kT \ln j + kT \ln \bar{v}\rho - \mu_{SR}$$

$$\mu_{PV} = -6kT \ln\frac{kT}{h\nu_E}$$

$$\mu_{NV}(j) = \mu_{PV} + [1 - \delta(j)]\mu_{NS}$$

Rotational and translational entropies were calculated using ideal gas formulae (34, 35) with the following quantities: k is Boltzmann's constant, T is the absolute temperature in °K, M is the mass of the hemoglobin monomer, and h is Planck's constant. I is the moment of inertia of the hemoglobin molecule and is calculated using the formula for spheres $I = 2/5\, MR^2$. The radius of the hemoglobin molecule in solution is taken to be 2.86×10^{-7} cm, calculated from its mass using a specific volume, $\bar{v}$, of 0.92 cm^3/g (15). The moment of inertia of the nucleus containing j molecules, $I(j)$ was calculated using the same expression with $M(j) = jM$ and the radius calculated from the mass using the polymer density, ρ, of 0.69 g/cm^3 (30). μ_{ST} is calculated for a standard state of 1 mM hemoglobin at infinite dilution, hence, $N_0 = 6.023 \times 10^{20}$, $V_0 = 10^3$ cm^3. Vibrational entropies were calculated using the Einstein lattice model (34, 35). The high temperature limit to the vibrational entropy is justified by the fact that the effective Einstein frequency, ν_E, which includes both center of mass and torsional "lattice" vibrations, is chosen to be 0.1 cm^{-1} in fitting the kinetic data. The form for the nucleus vibrational chemical potential, μ_{NV}, assumes only molecules with missing contacts have altered vibrational frequencies (see reference 28 for elaboration of this point).

effects in the nucleus. All other contributions to the equilibrium constants are calculated from standard statistical thermodynamic relations, are calculated from the structure of the polymer, or are known from experiment. The calculations are, of course, only approximate, but provide a good starting point for describing the free energy barrier to polymer formation.

The remaining parameters to be specified in Eqs. 6a and 6b are the polymerization and depolymerization rate constants, k_+ and k_-, and the scale factor ϕ. The value of k_- can be calculated from the relation $k_- = k_+\gamma_s c_s$ for a given value of k_+. There are, then, a total of five free parameters contained in our kinetic model.

For a given set of the five parameters and a value for the solubility, the coupled differential Eqs. 6a and 6b were numerically integrated to yield the monomer and polymer concentration as a function of time. To allow the nucleus size and nucleation equilibrium constants to vary with monomer concentration during the course of the polymerization, the expressions for the activities of the aggregates as a function of aggregate size (see Appendix) were analytically differentiated to solve for the size of the critical nuclei, $(n - 1)$ and $(m - 1)$. Using these values, the nucleation equilibrium constants K_N and K_M, could be reevaluated at each step of the integration.

Thus far we have carried out only a sufficient number of calculations to test the plausibility of the model. Parameters were chosen which had physically acceptable values, could generate experimentally measured tenth-times for a given initial supersaturation (c_0/c_s), and could also generate both a high concentration dependence on the tenth-times and a high time

dependence in the progress curves. Subsequently, parameters were selected by a trial and error procedure, which could also produce a decrease in both the concentration dependence and time dependence with increasing initial concentration.

The results of two extremes of a series of such calculations, performed as a function of initial monomer concentration, are shown in Fig. 8. The concentration used in the calculation of Fig. 8 *a* was 32.04 g/dl and for Fig. 8 *b* the concentration was 20.47 g/dl. The tenth-times calculated for these two concentrations were 7.64×10^{-3} and 2.74×10^{4} s. These results yield an average concentration dependence of ~34th order. The dependence of the tenth-time on the concentration for these parameter values is shown in more detail in Fig. 9 *a*. In agreement with the experimental data, the calculated dependence of the tenth-time on concentration decreases as the concentration increases. The calculated slopes are 56 at a concentration of 20.9 g/dl and 28 at a concentration of 32 g/dl. The decrease in slope is comparable to that seen in Fig. 4 which decreases from 21–26 at a concentration of 25.1 g/dl to 13–17 at a concentration of 38 g/dl. The decreased concentration dependence with increasing concentration results from a decrease in the size of both homogeneous and heterogeneous nuclei. For the longest tenth-time in Fig. 9, calculated for a supersaturation (c_0/c_s) of 1.15, the values of n and m are 46.3 and 32.3. For the shortest tenth-time in Fig. 9, corresponding to a supersaturation of 1.8, n has decreased to 7.9 and m to 5.5.

The progress curve in Fig. 8 *b* shows that the addition of heterogeneous nucleation to the model is also capable of generating the high time dependence which is observed in experiments on large volumes ($>10^{-4}$ cm^3) for delay times $\gtrsim$100 s. The time dependence of the calculated curve is 13.5, in good agreement with experimentally observed values of 10–20 for tenth-times of $\sim 10^4$ s (29). Fig. 8 *a* shows that the model also predicts the decrease in the time dependence of the progress curves which is seen for short tenth-times. The decrease in the time dependence results from the fact that the homogeneous nucleation pathway is more concentration dependent than the heterogeneous nucleation pathway for the formation of polymers. As the concentration increases the homogeneous path produces a larger and larger fraction of the total polymers present, thereby reducing the autocatalysis which results from heterogeneous nucleation and reducing the observed time dependece. Using the parameters

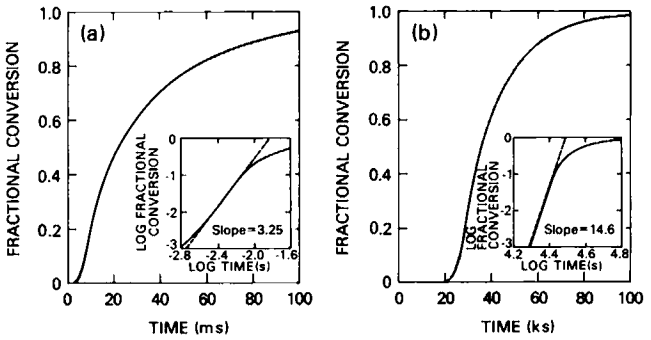

Figure 8 Calculated progress curves. The fractional extent of polymer formation is plotted as a function of time in milliseconds for a supersaturation of 1.7(*a*) and time in kiloseconds for a supersaturation of 1.15(*b*). The calculation was performed by integrating Eqs. 6a and 6b using the parameters: $\mu_{TR} - \mu_{PV} = 6$ kcal/mol, $\mu_{NS} = 3$ kcal/mol, $k_+ = 10^6 \text{M}^{-1}\text{s}^{-1}$, $\phi = 10^{-3}$, $c_s = 17.8$ g/dl, $T = 293°$K, $k_- = k_+\gamma_s c_s = 1.26 \times 10^4\ \text{s}^{-1}$, $A' = 1.15$. The curves have been normalized by dividing by the total amount of polymer present at equilibrium. In the insets, the logarithm of the fractional conversion has been plotted as a function of the logarithm of time. Linear fits to the calculated points for $10^{-2} < f < 10^{-1}$ yielded slopes of 3.25 (*a*) and 14.6 (*b*).

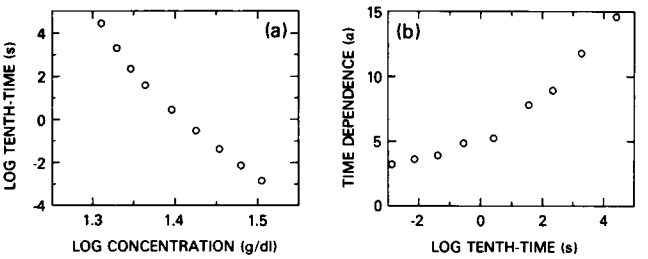

Figure 9 Concentration and time dependence of calculated progress curves. In (*a*) the calculated tenth-time is plotted on a log scale as a function of the logarithm of the total hemoglobin concentration. The plot yields a slope of 56 at log $c = 1.32$ and a slope of 28 at log $c = 1.50$. In (*b*) the slopes of log f versus log t plots (see Fig. 8) are shown as a function of the logarithm of the tenth-time.

given in Fig. 8, the slope of the theoretical time dependence decreases to 3.25 for a tenth-time of 7 ms. A more detailed look at the time dependence derived from the theoretical model is shown in Fig. 9 *b*.

The model can also explain the stochastic nature of the kinetics observed using the photolysis technique at times >10 s. At a supersaturation (c_0/c_s) of 1.3, using the parameters described in Fig. 8, primary nucleation produces 1.7×10^7 polymers per cm^3/s. Hence, in the (10^{-9} cm^3) volume of the photolysis experiment, only one polymer is predicted to be formed in 50 s. Since the tenth-time predicted by the model for this supersaturation is only 40 s, this simple calculation predicts that the observed events in a volume of 10^{-9} cm^3 should be significantly altered by the random variations in the time at which the nucleus will appear. Once nucleated, this polymer will grow to the size of the illuminated area (30 μm) in ~3 s and, using the rate for heterogeneous nucleation which was used for the simulation, the presence of this polymer will make the probability for heterogeneous nucleation about 5 times as great as that for a second primary nucleation event within the illuminated volume. It is thus highly likely that the remainder of the domain will polymerize by way of the heterogeneous pathway only. The small probabilities predicted for primary nucleation in the volumes of 10^{-9} cm^3 is thus completely consistent with the observed data. Slow experiments in which single domains are formed thus provide us with a new and totally independent means of determining the rate constant for the homogeneous nucleation event.

It should be clear from the preceding discussion that we have not yet attempted to carry out a rigorous fit of the model to kinetic data but have been interested primarily in testing its plausibility and exploring its capabilities at a qualitative level. The results thus far are extremely encouraging. The limited calculations presented here show that a model based on homogeneous and heterogeneous nucleation of polymers is capable of rationalizing the major results on the gelation of deoxyhemoglobin S, namely, the high concentration dependence of the tenth-time, the decrease in the concentration dependence with increasing initial concentration, the high time dependence observed for progress curves with long tenth-times, and the stochastic behavior of the tenth-times for the formation of single domains of polymers. While we have not yet performed detailed calculations, it is apparent from the relation between the equilibrium constants for nucleation (Eqs. A7 and A8) and the solubility that the model is also capable of explaining the high solubility dependence of the tenth-time (Eq. 1). Since the activation energy is dominated by the positive thermodynamic enthalpy change, which is given by the temperature dependence of the solubility, it appears that the model will rationalize the decrease in the activation energy with increasing temperature as well.

Several other observations on gelation kinetics are consistent with the prediction of the

model that gelation, when it occurs slowly, is initiated by homogeneous nucleation, but that the pathway for polymer formation rapidly becomes dominated by heterogeneous nucleation. Progress curves from light scattering experiments, in which the appearance of polymer could be followed for nearly five decades of signal change, showed almost purely autocatalytic behavior. Moreover, when gels have been melted by cooling and regelled after observable birefringence or scattering signals have disappeared, the regelation progress curves are identical to the original gelation progress curves except for a decrease in the tenth-time (36). This experiment again suggests that gelation can be initiated by an undetectable fraction of the hemoglobin still existing as polymers, and is, therefore, consistent with the notion that gelation is initiated by the homogeneous nucleation of a very small number of polymers. The present calculations, in fact, suggest that the formation of a single domain is associated with a single homogeneous nucleation event. This suggestion could explain the long-standing observation that the number of domains observed in gelled samples is approximately linearly proportional to the reciprocal tenth-time. The domain densities observed in thin samples, using linear birefringence to resolve individual domains, vary from a few domains per square millimeter for gels formed with tenth-times of 10^5 s to many domains per square micrometer for samples gelled in milliseconds. The density of domains therefore increases by more than a factor of 10^6 as the tenth-times decrease by about a factor of 10^7.

In addition to synthesizing a large amount of information on gelation kinetics, the model is also valuable because it can be further tested by a number of key experiments. The most telling would be the complete characterization of the distribution of progress curves for single domain formation in slowly gelling samples using our photolysis technique. This data will provide both absolute values for the rate of homogeneous nucleation and values for the concentration dependence of the heterogeneous nucleation process. The model also predicts that polymers grow in an intrinsically ordered array and that alignment of polymers is not subsequent, but simultaneous with their formation. Simultaneous measurements of birefringence and light scattering at high sensitivity should allow a detailed test of this requirement. The model can also be tested by time-resolved electron microscopy, as it predicts both the average polymer lengths and the time dependence of this average.

Finally, we should point out that further theoretical development of this model should include a more rigorous treatment of several aspects of the problem, including variation of the parameters over a wide range of values, estimates of the activity coefficients for the nucleus and other small post-nuclear aggregates, and more accurate calculations of the equilibrium constants for both homogeneous and heterogeneous nucleation.

We thank David Felsenthal for considerable assistance with the numerical analysis of the experimental data.

APPENDIX

Calculation of Equilibrium Constants for Nucleus Formation

To develop an expression for the equilibrium constants for the formation of the critical nuclei, we turn to the theories of nucleation which have been developed for the condensation and crystallization of small molecules (27, 28, 33). In these theories the formation of large aggregates proceeds via monomer addition to smaller aggregates. The small aggregates, because of their larger surface/volume ratios, are less stable than the final bulk phase and this thermodynamic instability acts as a barrier to the formation of the condensed phase. For hemoglobin S gels, we can write the chemical potentials of the polymer and

solution phases, μ_S and μ_P, as

$$\mu_S = \mu_S^0 + kT \ln \gamma c,$$
$$\mu_P = \mu_P^0, \tag{A1}$$

where μ_S^0 and μ_P^0 are the standard state chemical potentials of the monomer in the solution and polymer phases, respectively. At solubility equilibrium, $\mu_S = \mu_P$ and

$$RT \ln \gamma_s c_s = \mu_P^0 - \mu_S^0, \tag{A2}$$

where the subscript s refers to the solubility equilibrium conditions. We assume that rotational and translational motions of the entire protein molecule are separable from the internal degrees of freedom in the solution phase and that the lattice vibrations into which translations and rotations are converted are also separable in the polymer phase. We can then use the classical translational and rotational partition functions for an ideal gas to estimate the contribution to the monomer chemical potential from these terms, and the Einstein lattice model to estimate the contribution from the vibrations to the polymer chemical potential. With these assumptions, we can write

$$\mu_S^0 = \mu_{ST} + \mu_{SR} + \mu_{SI}$$
$$\mu_P^0 = \mu_{PV} + \mu_{PC} + \mu_{PI}, \tag{A3}$$

where μ_{ST}, μ_{SR}, and μ_{PV} are given in Table I. The intermolecular bonding (contact) contribution to the polymer chemical potential is denoted by μ_{PC} and the contribution from the internal modes of the protein by μ_{SI} and μ_{PI} in the solution and polymer phases, respectively.

To describe the chemical potential of a nucleus containing j monomers, we introduce the function $\delta(j)$ which describes the ratio of the number of contacts per monomer in the aggregate of j molecules to the number of contacts per monomer in an infinite polymer. We then have

$$\mu_N(j) = j\{\delta(j)\mu_{PC} + \mu_{PV} + \mu_{NI} + [1 - \delta(j)]\,\mu_{NS}\} + \mu_{NR} + \mu_{NT} - \mu_{PV} + kT \ln \gamma_N c_N, \tag{A4}$$

where μ_{NI} is the contribution to the chemical potential from the internal modes of the molecules in the nucleus and $[1 - \delta(j)]\mu_{NS}$ is the difference between the vibrational contribution to the chemical potential of the nucleus and that of the the same j molecules in the infinite polymer. μ_{NR} and μ_{NT} are the contributions to the nucleus' chemical potential resulting from its own translational and rotational degrees of freedom and are also given in Table I. To determine the concentration of the j-mer present at equilibrium, we set $\mu_N(j) = j\mu_S$ and find:

$$kT \ln \gamma_N c_N = j\{kT \ln \gamma c/\gamma_s c_s + [1 - \delta(j)]\,(kT \ln \gamma_s c_s + \mu_{SR} + \mu_{ST} + \mu_{SI} - \mu_{PV} - \mu_{NS}) - [\mu_{NI} - \delta(j)\,\mu_{PI}]\} - \mu_{NT} - \mu_{NR} + \mu_{PV}. \tag{A5}$$

If the internal chemical potentials scale in the same way as the contributions from the intermolecular contacts, that is. if

$$\mu_{NI} - \mu_{SI} = \delta(j)(\mu_{PI} - \mu_{SI}), \tag{A6}$$

these terms can be incorporated into the contact free energies and vanish from Eq. A5. Using this result and the relations in Table I for μ_{NR} and μ_{NT} we have for K_N:

$$kT \ln K_N = (n - 1)\{[1 - \delta(n - 1)](\mu_{TR} - \mu_{PV} - \mu_{NS}) - kT\delta(n - 1) \ln \gamma_s c_s\} - \mu_{TR} + \mu_{PV} - kT[\ln \bar{V}\rho - 4 \ln (n - 1)], \tag{A7}$$

where $n - 1$ is the number of hemoglobin S molecules in the critical nucleus and we have defined $\mu_{TR} \equiv \mu_{ST} + \mu_{SR}$ to simplify the final expression. A similar treatment for the heterogeneous nucleation yields

$$kT \ln K_M = (m - 1)\{[1 - \delta'(m - 1)](\mu_{TR} - \mu_{PV} - \mu_{NS}) - kT\delta'(m - 1) \ln \gamma_s c_s\}, \tag{A8}$$

where $m - 1$ is the number of molecules in the heterogeneous nucleus. The function $\delta'(j)$ has been

modified from $\delta(j)$ to account for the presence of contacts which exist between the secondary nucleus and the surface of the existing polymer. Since the heterogeneous nucleus is attached to a polymer, we have neglected the contribution of translational and rotational free energy to its chemical potential.

The function $\delta(j)$ was determined by counting the number of contacts in compact, hexagonally close packed aggregates of size j and comparing the result with the number of contacts per monomer in a polymer having the structure described recently by Dykes et al. (16). The ratio was fit to the function:

$$\delta(j) = \frac{-A \ln j}{j} + 1 \tag{A9}$$

This gave a value of $A = 1.90$ and fit the computed numbers of $j = 4$–50 with an rms error of 0.015. The same functional form was used to describe $\delta'(j)$, but the parameter $A' < A$ was used since there are additional intermolecular bonds formed by the interaction of the heterogeneous nucleus with the existing polymer. Monomer activity coefficients were specified using:

$$ln\,\gamma = \sum_{i=2}^{6} 1/(i-1)\, B_i\, c^{i-1}, \tag{A10}$$

with the hard sphere values for the virial coefficients: $B_2 = 7.0$ V, $B_3 = 27.0$ V^2, $B_4 = 43.45$ V^3, $B_5 = 67.74$ V^4, $B_6 = 95.97$ V^5, and V = 0.92 cm^3/g (14, 15).

Received for publication 11 December 1979.

REFERENCES

1. Hercules, J. I., A. N. Schechter, W. A. Eaton, and R. E. Jackson, editors. 1974. Proceedings of the First National Symposium on Sickle Cell Disease. DHEW Publication No. (NIH) 75–723.
2. Hercules, J. I., G. L. Cottam, M. R. Waterman, and A. N. Schechter, editors. 1976. Proceedings of the Symposium on Molecular and Cellular Aspects of Sickle Cell Diseases. DHEW Publication No. (NIH) 76–1007.
3. Caughey, W. S., editor. 1978. Proceedings of the Symposium on Clinical and Biochemical Aspects of Hemoglobin Abnormalities. Academic Press, Inc., New York.
4. Hofrichter, J., D. G. Hendricker, and W. A. Eaton. 1973. Structure of hemoglobin S fibers: optical determination of the molecular orientation in sickled erythrocytes. *Proc. Natl. Acad. Sci. U.S.A.* **70**:3604.
5. Ross, P. D., J. Hofrichter, and W. A. Eaton. 1975. Calorimetric and optical characterization of sickle cell hemoglobin gelation. *J. Mol. Biol.* **96**:239.
6. Finch, J. T., M. F. Perutz, J. T. Bertles, and J. Dobler. 1973. Structure of sickled erythrocytes and of sickle cell hemoglobin fibers. *Proc.. Natl. Acad. Sci. U.S.A.* **70**:718.
7. Josephs, R., H. S. Jarosch, and S. J. Edelstein. 1976. Polymorphism of sickle cell hemoglobin fibers. *J. Mol. Biol.* **102**:409.
8. Garrell, R. L., R. H. Crepeau, and S. J. Edelstein. 1979. Cross-sectional views of hemoglobin S fibers by electron microscopy and computer modelling. *Proc.. Natl. Acad. Sci. U.S.A.* **76**:1140.
9. Briehl, R. W. 1978. Gelation of sickle cell hemoglobin. IV. Phase transition in hemoglobin S gels: separate measures of aggregation and solution-gel equilibrium. *J. Mol. Biol.* **123**:521.
10. Williams, R. C., Jr. 1973. Concerted formation of the gel of hemoglobin S. *Proc.. Natl. Acad. Sci. U.S.A.* **70**:1506.
11. Magdoff-Fairchild, B., W. N. Poillon, T. I. Li, and J. F. Bertles. 1976. Thermodynamic studies of polymerization of deoxygenated sickle cell hemoglobin. *Proc.. Natl. Acad. Sci. U.S.A.* **73**:990.
12. Hofrichter, J., P. D. Ross, and W. A. Eaton. 1976. Supersaturation in sickle cell hemoglobin solutions. *Proc.. Natl. Acad. Sci. U.S.A.* **73**:3035.
13. Ross, P. D., J. Hofrichter, and W. A. Eaton. 1977. Thermodynamics of gelation of sickle cell deoxyhemoglobin. *J. Mol. Biol.* **115**:111.
14. Ross, P. D., and A. P. Minton. 1977. Analysis of non-ideal behavior in concentrated hemoglobin solutions. *J. Mol. Biol.* **112**:437.
15. Ross, P. D., R. W. Briehl, and A. P. Minton. 1978. Temperature dependence of nonideality in concentrated solutions of hemoglobin. *Biopolymers.* **17**:2285.
16. Dykes, G., R. H. Crepeau, and S. J. Edelstein. 1978. Three dimensional reconstruction of the fibers of sickle cell hemoglobin. *Nature (Lond.).* **272**:506.

17. Magdoff-Fairchild, B., and C. C. Chiu. 1979. X-ray diffraction studies of fibers and crystals of deoxygenated sickle cell hemoglobin. *Proc. Natl. Acad. Sci. U.S.A.* **76**:223.
18. Nagel, R. L., and R. M. Bookchin. 1978. Areas of interaction in HbS polymer. *In* Proceedings of the Symposium on Clinical and Biochemical Aspects of Hemoglobin Abnormalities. W. S. Caughey, editor. Academic Press, Inc., New York. 195.
19. Hofrichter, J., P. D. Ross, and W. A. Eaton. 1974. Kinetics and mechanism of deoxyhemoglobin S gelation: a new approach to understanding sickle cell disease. *Proc.. Natl. Acad. Sci. U.S.A.* **71**:4864.
20. Malfa, K., and J. Steinhardt. 1974. A temperature-dependent latent period in the aggregation of sickle cell deoxyhemoglobin. *Biochem. Biophys. Res. Commun.* **59**:887.
21. Moffat, K., and Q. H. Gibson. 1974. The rates of polymerization and depolymerization of sickle cell hemoglobin. *Biochem. Biophys. Res. Commun.* **61**:237.
22. Harris, J. W., and H. B. Bensusan. 1975. The kinetics of the sol-gel transformation of deoxyhemoglobin S by monitoring viscosity. *J. Lab. Clin. Med.* **86**:564.
23. Eaton, W. A., J. Hofrichter, P. D. Ross, R. G. Tschudin, and E. D. Becker. 1976. Comparison of sickle cell hemoglobin kinetics measured by NMR and optical methods. *Biochem. Biophys. Res. Commun.* **69**:538.
24. Kowalczykowski, S., and J. Steinhardt. 1977. Kinetics of hemoglobin S gelation followed by continuously sensitive low-shear viscosity. *J. Mol. Biol.* **115**:201.
25. Hofrichter, J., P. D. Ross, and W. A. Eaton. 1976. A physical description of hemoglobin S gelation. *In* Proceedings of the Symposium on Molecular and Cellular Aspects of Sickle Cell Disease. J. I. Hercules, G. L. Cottam, M. R. Waterman, and A. N. Schechter, editors. DHEW Publication No. 76–1007, 185–222.
26. Noguchi, C. T., and A. N. Schechter. 1977. Effects of amino acids on gelation kinetics and solubility of sickle hemoglobin. *Biochem. Biophys. Res. Commun.* **74**:637.
27. McDonald, J. E. 1962. Homogeneous nucleation of vapor condensation. I. Thermodynamic aspects. *Am. J. Phys.* **30**:870.
28. Abraham, F. F. 1974. Homogeneous nucleation theory. Academic Press, Inc., New York.
29. Eaton, W. A., and J. Hofrichter. 1978. Successes and failures of a simple nucleation theory of sickle cell hemoglobin gelation. *In* Proceedings of the Symposium on Clinical and Biochemical Aspects of Hemoglobin Abnormalities. W. S. Caughey, editor. Academic Press, Inc., New York. 443.
30. Sunshine, H. R., J. Hofrichter, and W. A. Eaton. 1979. Gelation of sickle cell hemoglobin in mixtures with normal adult and fetal hemoglobin. *J. Mol. Biol.* **133**:435.
31. Ferrone, F. A., J. Hofrichter, and W. A. Eaton. 1978. Hemoglobin S polymerization in the photostationary state. *In* Frontiers of Biological Energetics: From Electrons to Tissues. Vol. II. P. L. Dutton, J. S. Leigh, and A. Scarpa, editors. Academic Press, Inc., New York. 1085.
32. Hofrichter, J. 1979. Ligand binding and the gelation of sickle cell hemoglobin. *J. Mol. Biol.* **128**:335.
33. Zettlemoyer, A. C. 1969. Nucleation. Marcel Dekker, New York.
34. Hill, T. 1960. An Introduction to Statistical Thermodynamics. Addison-Wesley, Reading, Massachusetts.
35. Lewis, G. N., M. Randall, K. S. Pitzer, and L. Brewer. 1961. Thermodynamics. McGraw Hill, New York.
36. Hofrichter, J., J. S. Gethner, and W. A. Eaton. 1978. Mechanism of sickle hemoglobin gelation. *Biophys. J.* **24**:20 (Abstr.).

DISCUSSION

Session Chairman: Alan Schechter *Scribe*: John J. Steckert

HERZFELD: I have a question on birefringence measurements. Your results for single domain samples suggest that polymers grow in an intrinsically ordered array rather than aligning after formation. However, measurements of large, thermally induced gels show that birefringence continues to increase after polymerization is essentially finished as measured by turbidity, water proton magnetic relaxation, and calorimetry. Would you compare your results with those for the large thermally-induced gels, and would you explain the difference?

FERRONE: In the data you refer to, of course, the bulk of the birefringence curve does correspond to the same kind of curve that one sees from, e.g., calorimetry, though there is a slow continued increase. That increase would not contradict our model. What we stress is that alignment and growth are simultaneous not necessarily that all alignment is complete at the end of growth. In these multi-domain samples one domain could be growing at the expense of another. Alternatively, there is the possibility of domains themselves annealing further. We don't have any complete explanation.

Let me emphasize that our work is concentrating on the first 10% of the reaction curves. What happens at the end may be domain impingement or something that has yet to be discovered.

HERZFELD: Another question, on heating effects: Absorption of light and consequent heating would be expected to be strongest in regions of high hemoglobin concentration. Your initial monomer solutions are uniform. However, since a polymer is a highly concentrated form of hemoglobin in and of itself, you could conceivably get local heating. If you have a hot zone around the polymer, is there the possibility of getting fast polymerization along the polymer due to that heating effect? Can you exclude that phenomenon as an explanation for the apparent heterogeneous catalysis?

FERRONE: Yes, I think we can exclude that by three separate lines of reasoning. First, a simple numerical calculation suffices to demonstrate that what you suggest is unlikely. The kind of heating on account of the laser is something like 4° above the outside ambient solution. So if one takes a linear gradient from, say, the center of the sample to the outside edge, and asks how much temperature gradient does that correspond to within the sample, say within the diameter of a fiber, one finds that we are talking ~0.05° per fiber diameter. That gradient is not very large. Further one needs not only a temperature gradient but also a rate that is temperature dependent. As our paper shows, the activation energy is temperature dependent itself: there are regions where there is no change in rate for a small change in temperature, and even in those regions we see evidence of this secondary phase. That is the first line of reasoning.

Our second line of reasoning is that in this model (Eq. (6*a*) and (6*b*) of our paper) it is necessary to have n and m differ in order to be able to account for the different concentration dependence at the two ends of the regions we studied. If the heterogeneous part were totally due to just a thermal effect, one would have a second term that was a nucleation term just like the first one. That second term would have the same exponent and one would not be able to fit the changing concentration dependence of the data.

Our third reason, and let me stress this, is that the heterogeneous part is what we are invoking to explain the autocatalytic behavior that everyone has seen up until now. In other words our experiments, as we interpret them, are the first ones in hemoglobin that have actually observed homogeneously dominated nucleation. Hence this new term might even have been introduced as a way to explain the sharpness of the curves in previous experiments, not just ours with the laser.

ENGLANDER: I am a little worried about some of the data that you show in Fig. 4 which seem to differ importantly from some of my preconceptions and from some of our results. In the range of low HbS concentration there is a difference in the absolute rate of nucleation, which appears to be a hundred times too slow, and also there is a clear discrepancy in the dependence of rate on concentration, which decreases rather than increases as I had always thought it should.

FERRONE: Can you restate that discrepancy in the absolute rate?

ENGLANDER: From what Ross and Minton and Behe and I have said, as you go up in concentration the rate of nucleation should increase rapidly, that is, the dependence of rate on concentration should increase so your line should slope down, should get steeper rather than flatter.

FERRONE: That is only the activity contribution to the rate. Our calculations took that variation in activity into account as well as the change in nucleus size. *A priori* it is anyone's guess as to whether activity or the change in nucleus size will dominate. One has to sit down and do a calculation or make the measurements.

ENGLANDER: I understand that you can write the kind of theory you talked about which will rationalize the observations and find self-consistency. However, we have data which suggest that the nucleus size does not change over the range of concentration from 15% clear up to ~27%. I have tried to think about possible artifacts. An interesting one occurred to me and since it refers to your experiment rather than ours, I thought you might like to hear about it. In the range of 30% or so concentration, your heme concentration is ~20 mM, and so is the bound CO. At time zero of your experiments you turn on your laser and flash off all that CO, which presumably goes into solution. In other words you start off with 20 mM concentrations of CO, equal to 20 atm partial pressure of CO. Where does that CO go? Let us assume that there is something to what Frauenfelder and Lakowicz and Weber have been talking about. At 20 mM CO concentration the average distance between CO molecules is something like 35 Ångstroms. If you take a hemoglobin molecule and plunk it down into that solution, it will intersect one or two CO molecules. So you now have to consider the interesting possibility that in your experiments, once you flash, though you have proved that the CO is not bound to the heme iron there may be significant CO actually inside the body of the molecule. Frauenfelder has compared this situation to a camel in a tent. The internal CO may distort the hemoglobin molecule and therefore to some extent produce hemoglobin S inactive with respect to the polymerization reaction. That would account for both discrepancies I've mentioned. For example, as you go to higher concentrations where you get more

and more CO into solution, you get higher and higher fractional inactivation of hemoglobin S and therefore you find a tailing-off of the concentration dependence, and in general you find low rates.

FERRONE: What is not immediately clear is what sign or what magnitude any such predictions would have to have. After all we are talking about having at most one CO lost somewhere within one subunit of the hemoglobin molecule for the times you mention. We know, of course, that the CO has not stayed in the heme pocket; otherwise it would rebind in times that are trivially short. In a set of measurements which we have done as a control experiment to calculate diffusion constants of CO through the protein solution, we get within a factor of two of published CO diffusion constants for concentrated protein solutions. So if there is some bizarre effect here it is the "normal" bizarre effect that happens when one has concentrated solutions. I am not sure that you can say that CO is caught in the protein or is causing any effect. In the red cell one has these high concentrations and, presumably if CO or oxygen likes to diffuse through the protein, it may well be doing that in the normal physiological conditions.

ENGLANDER: You never have 20 mM of ligand free in any solution. Also you would not see this in free solution diffusion experiments. According to what Lakowicz and Weber tell us, CO may run in and out of proteins at a diffusion limited rate. So the protein would not interfere with diffusion.

WISHNIA: Dr. Englander raises an interesting question. There is a hydrophobic binding site on hemoglobin, which is not particularly where the hydrophobic binding site is on myoglobin. It is somewhere between the EF and GH corners of hemoglobin. It's the place where xenon goes and the place where pentane goes and there is probably no reason in the world why, at 20 mM, CO should not go there. An old report of Murayama's said that propane will unsickle hemoglobin, and it is conceivable that depending on the CO concentration you will get variable degrees of unsickling.

FERRONE: Let us bear in mind that one is not talking about an equilibrium effect. We see that the CO does leave the reaction volume in times that, as far as we can tell, are for these solution conditions diffusion controlled. If there is any kind of a site it would weakly bind temporarily and not give rise to long term binding.

Secondly, a binding site would have an effect on the slower experiments too at these concentrations, and yet our data agree with thermally induced data at comparable times. So all these effects of a binding site can be categorically ruled out because we know the CO is leaving and we know that the slow time behavior is correct.

MINTON: You might want to consider two effects which may prove significant. First, we are accustomed to treat the system as two phases; we think of a solution phase and a polymer phase, and we treat these as thermodynamic phases. We know that the polymer "phase" is really not a true, stable thermodynamic phase. I would think that at the very beginning of this polymerization reaction, where you have just started to build these domains, the chemical potential of the hemoglobin molecule in the so-called polymer phase may depend on the size of the domain and thereby be a function of time. You might want to consider the kinetics of annealing the polymer as it grows and stabilizes.

The second point is in connection with the proposed mechanism of heterogeneous nucleation. You have considered in at least this first-order model that the number of surface sites is proportional to the number of polymerized hemoglobin molecules. If these domains are as dense as we believe they are, then the accessibility of the putative surface sites would probably be a function of the domain size. In the second term of Eq. (*6a*) and (*6b*), where you have the $(c_o\text{-}c)$, which is supposed to be proportional to the number of heterogeneous nucleation sites, I would suggest that probably in a more general sense you might want to use a $(c_o\text{-}c)$ raised to an exponent and that exponent would be less than one, with its value a function of the size of the domain. In the limit that the domain is extremely close packed, that exponent would be 2/3.

FERRONE: To respond to the question of whether or not we should take the polymer state as being ambiguously determined, necessitating taking its order into account, another way of phrasing that would be to say that the solubility then depends upon the degree of order that one has in a given sample. The degree of order we have seen here, as in other cases, is reflected in the speed with which polymerization occurs. All of the experiments done to date show that the solubility does not depend upon how fast or how slowly one did the experiment. To a very good approximation that additional term arising from order, that additional free energy, is going to be small—probably ultimately needed, but small nevertheless.

As for the second question, let us recall we are dealing with only the case of the first 10% of the reaction. A quantity raised to the two-thirds power is not going to differ much from linear behavior in a first approximation. Our assumption that polymers are long, linear, and dilute is still probably valid over the region of our modeling, but when we try to complete the model we will want to take into account some kind of exclusion. For now this is close enough to let us continue with this kind of calculation.

MINTON: The "equilibrium" solubilities (or what we consider to be equilibrium solubilities) are measured in "equilibrium" between soluble hemoglobin and a well-formed macroscopic condensed phase that has been around for

quite awhile because we let this process come to an equilibrium or at least a steady state. What you are talking about, the ordering, may have come to some kind of an asymptotic level in the long time limit. I'm talking about something that is taking place at very short times and it may not be comparable.

FERRONE: We can't tell yet whether or not for the extremely short times that kind of order would result in a change of solubility.

B. K. LEE: Obviously there are many mechanisms that could explain the fact that the rate of nucleation increases as the nucleation process goes on. Your mechanism is one of them. I have assumed in the past that, in the case of nucleation of crystals from solution, the following two mechanisms would be important. One, as one nucleation site grows it breaks and produces two or more new nucleation sites. Two, heat is generated when a solute species deposits on the surface of the condensed phase and that this produces convections and turbulences in the solution, disturbing the supersaturated, metastable state of the solution.

FERRONE: We tried a number of mechanisms that appeared to us to be simple and plausible, and excluded all but the one here. In particular we excluded the model of fragmentation whereby polymers were growing and breaking and thus providing an increased number of ends. That model just did not have all of the characteristics that we needed to describe the available data; in particular it had too low a concentration dependence. There may be some other way of describing a nucleation mechanism than the one we have described. Ours pins itself to a number of observed phenomena that allow us to have faith in it beyond just having a set of curves fit by a set of parameters.